Phase diagram of the dipolar Ising ferromagnet on a kagome lattice

Hisato Komatsu,[1,*] Yoshihiko Nonomura ,[2,†] and Masamichi Nishino [1,3,‡]
[1]*Research Center for Advanced Measurement and Characterization, National Institute for Materials Science, Tsukuba, Ibaraki 305-0047, Japan*
[2]*International Center for Materials Nanoarchitectonics, National Institute for Materials Science, Tsukuba, Ibaraki 305-0044, Japan*
[3]*Elements Strategy Initiative Center for Magnetic Materials, National Institute for Materials Science, Tsukuba, Ibaraki 305-0047, Japan*

(Received 20 February 2022; revised 30 May 2022; accepted 27 June 2022; published 6 July 2022)

We study the field-temperature phase diagram of the two-dimensional dipolar Ising ferromagnet on a kagome lattice with a specific ratio between the exchange and dipolar constants, $\delta = 1$. Using the stochastic cutoff $O(N)$ Monte Carlo method, we calculated order parameters for stripe and bubble phases and other thermodynamical quantities. We find two kinds of stripe phases at low fields, where the arrangement of the branch spins neighboring the stripe frame varies, and two bubble phases at high fields, in which three-spin domains (bubbles) form a regular triangular lattice but the triangular array of bubbles changes on the kagome lattice. We also find that with increasing field, a disordered phase exists between the stripe and bubble phases and between the two bubble phases. We discuss the details of the features of these phases and phase transitions.

DOI: 10.1103/PhysRevB.106.014402

I. INTRODUCTION

Magnetic thin films have attracted much attention because of applications for high-density magnetic recording [1,2]. In such systems the competition between short-range exchange and long-range dipolar interactions with the influence of other interactions causes rich magnetic structures. For example, with magnetocrystalline anisotropies, various stripe patterns appear, and spin-reorientation (SR) transitions take place [3–7], and with Dzyaloshinskii-Moriya interactions, helical structures and skyrmions are formed [8].

In ferromagnetic films, a characteristic phenomenon has often been observed experimentally with increasing external magnetic field. A stripe phase at low fields changes to a phase called the "bubble phase" before a transition to a ferromagnetic phase at high fields. In the bubble phase, magnetic domains are arranged almost periodically, forming a triangular lattice [9–11].

The properties of the stripe and bubble phases have also been theoretically studied by magnetostatic approaches [9,10], coarse-grained effective free-energy approaches such as Ginzburg-Landau theory [12–14], and lattice models [14,15]. In the magnetostatic approaches, the magnetostatic energies were compared between the structures of a parallel-stripe array and cylindrical domains, and a field-thickness phase diagram without a thermal effect was studied [9,10]. In the effective free-energy approaches, the phase boundaries between the stripe and bubble phases and between the bubble and uniform (ferromagnetic) phases were investigated. A first-order transition was suggested for the former [12,14], while a Berezinskii-Kosterliz-Thouless (BKT)-like transition [16,17] was pointed out for the latter [12], in which a bubble melting transition, i.e., dislocation unbounding, occurs in a manner similar to two-dimensional (2D) melting transitions [18–20]. These coarse-grained approaches can treat large systems, but they were based on the mean-field theory, and the thermal fluctuation effect was insufficiently treated. In addition, periodic structures were assumed for the stripe and bubble phases, and the stabilities of the two phases were compared.

On the other hand, in the lattice model approaches using 2D dipolar Ising and Heisenberg ferromagnets, which treat the thermal fluctuation effect precisely using Monte Carlo (MC) methods, such periodic structures are spontaneously formed without the assumption of the periodicity. However, it is difficult to simulate models with large sizes. Because of the long-range nature of the dipolar interaction, $O(N^2)$ (N is the total number of spins) computational time, namely, a high computational cost, is required. Stripe phases and SR transitions have been investigated in several parameters of the 2D dipolar Ising [21–34] and Heisenberg [35–50] ferromagnets, but studies on the stripe-bubble and bubble-ferromagnetic transitions are limited [14,15]. In these studies on square lattices, the intermediate phase located between (anharmonic) stripe and saturated ferromagnetic phases was named the bubble phase, in which domains were observed. However, the formation of any lattice structure of the domains was not studied and is unclear. A first-order transition was indicated between the stripe and bubble phases, and BKT-like melting behavior was suggested between the bubble and saturated ferromagnetic phases [15].

In the present paper, we investigate the properties of the stripe and bubble phases and phase transitions in the 2D dipolar Ising ferromagnet on a kagome lattice. Kagome lattice systems have been intensively studied in relation to spin liquids. Geometrical frustration arises in antiferromagnetic

*komatsu.hisato@nims.go.jp
†nonomura.yoshihiko@nims.go.jp
‡Corresponding author: nishino.masamichi@nims.go.jp

interactions in these systems and also arises in ferromagnetic interactions with local anisotropies such as spin ice, in which the constraint of an icelike rule causes macroscopic degeneracy [51]. Recently, kagome dipolar spin-ice systems were artificially prepared, and whether or not the dipolar interaction, i.e., long-range interaction, influences the local spin state is a topic of study [52,53]. The kagome-lattice pure dipolar Heisenberg model was also investigated, and ferromagnetic orders by planer spins at zero field were shown [54,55].

We focus on the effect of defects of a kagome lattice on magnetic structure. A kagome lattice is obtained by removing $1/4$ of the sites forming a triangular lattice with a spacing of $2a$ from a triangular lattice with lattice constant a. Periodic defects exist. We study whether or not defects affect the properties of stripes and bubble phases in a dipolar Ising ferromagnet, which is our motivation for this study.

According to the studies using the effective energy approaches, we define an order parameter for bubble phases to detect a lattice on which magnetic domains are arranged. We estimate several order parameters using a MC method and study the field-temperature phase diagram with a specific ratio between the exchange and dipolar constants, $\delta = 1$.

To overcome the difficulty of the $O(N^2)$ computational time required for conventional MC algorithms, we use the stochastic cutoff (SCO) $O(N)$ MC method [56] to reduce the computational cost. We show two stripe phases at low fields and two bubble phases at high fields and present a disordered phase between the stripe and bubble phases, between the two bubble phases, and above the higher-field bubble phase. We also discuss the phase transitions associated with these phases. The argument about the previously suggested BKT-like melting behavior is beyond the scope of the present work because it is a delicate issue which requires huge computations to obtain a convincing result.

The rest of this paper is organized as follows. In Sec. II, the model and method are presented. In Sec. III, the results and discussion are given. After an overview of the field-temperature phase diagram in Sec. III A, the features of the bubble phases and stripe phases are discussed in Secs. III B and III C, respectively. The properties of the phase transitions are studied in Sec. III D. Section IV is devoted to the summary.

II. MODEL AND METHOD

We consider an Ising spin system on a kagome lattice in the xy plane (Fig. 1). The position of the ith spin in units of the lattice constant is given as

$$\left(\mu_i + \frac{1}{2}\delta_{1,\,(\nu_i \bmod 2)}, \frac{\sqrt{3}}{2}\nu_i\right), \tag{1}$$

where $\delta_{m,n}$ is the Kronecker delta and μ_i is integer if $\nu_i \bmod 4 = 1$ or 3, odd if $\nu_i \bmod 4 = 0$, and even if $\nu_i \bmod 4 = 2$. The Hamiltonian of the system consists of the nearest-neighbor ferromagnetic Ising interaction, dipolar interaction, and Zeeman term:

$$\mathcal{H} = -\delta \sum_{\langle i,j \rangle} \sigma_i \sigma_j + \sum_{i<j} \frac{\sigma_i \sigma_j}{r_{ij}^3} - H \sum_i \sigma_i. \tag{2}$$

Here, σ_i is $\sigma_i = 1$ (up spin) or -1 (down spin), perpendicular to the xy plane; $\delta(> 0)$ is the ratio between the exchange and dipolar constants; r_{ij} is the distance between the ith and jth spins; and H is the magnetic field parallel to the Ising spins. In this paper, we study the case of $\delta = 1$.

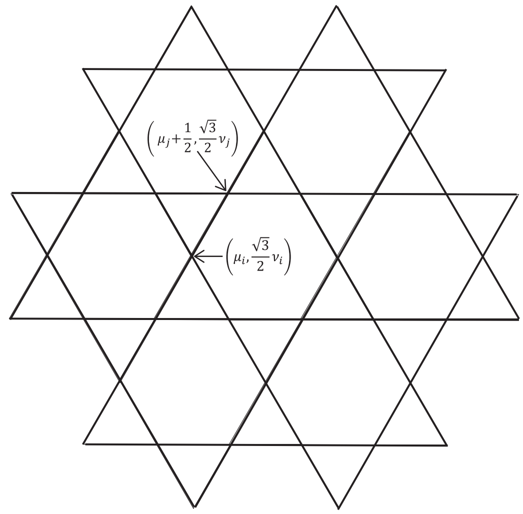

FIG. 1. Structure of the kagome lattice.

As mentioned in the Introduction, $O(N^2)$ simulation time is required in conventional MC methods, and we use the SCO $O(N)$ MC method [56] with the modification shown in the Appendix.

To estimate the H dependences of the order parameters at a given temperature T, a simulated annealing is performed starting from a random spin configuration at each H, i.e., gradual lowering of the temperature to the given T. For the T dependences of the order parameters at a given H, the temperature is lowered from a high temperature, except in the study of the hysteresis properties with respect to temperature in Figs. 13 and 14. For the hysteresis properties, in the heating process the temperature is increased starting from a configuration in the lower-temperature phase (bubble A or B), while in the cooling process the temperature is lowered staring from a configuration in the higher-temperature phase (disordered). At each T and H, 400 000 MC steps are used for the measurement of the order parameters after 100 000 MC steps for the equilibration, and the average of each order parameter is taken over 12 and 48 independent simulations for the H and T dependences, respectively.

To treat large systems and exclude the effect of edges, we tile replicas of the original system of $N = L^2 = 96\times96$ sites with periodic boundary conditions [31,32] as follows. We tile 2001×2001 replicas. We consider all interactions for a total of $96\times96\times2001\times2001$ sites in an area of $(2001L)^2$ under the condition of the same spin configuration in each replica. By introducing replicas, we treat the dipolar interaction of spin pairs at a long distance such as $1000L$. Throughout this paper, we use $k_B = 1$.

III. RESULTS AND DISCUSSION

A. Phase diagram

First, we give an overview of the structure of the phase diagram obtained in this study. The field-temperature (H-T) phase diagram is shown in Fig. 2. We find two bubble phases

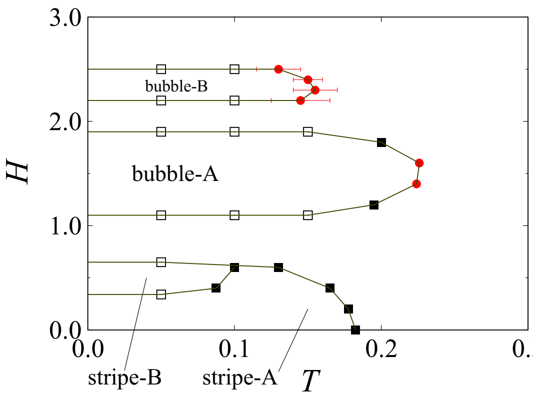

FIG. 2. H-T phase diagram of the system. The solid circles show the first-order transition points obtained by analyzing the energy histogram or thermal hysteresis property. The solid squares are transition points estimated by the heat capacity analysis. The open squares are transition points estimated by the H dependences of the order parameters. The error bars indicate the hysteresis widths.

at high fields. We call the bubble phases at lower and higher fields bubble phases A and B, respectively. Figures 3(a) and 3(b) show the magnetic structures in the space-filling configuration in bubble phases A and B, respectively. In both bubble phases, three nearest-neighbor down spins form a domain, i.e., bubble, and bubbles form a regular triangular lattice, but the triangular array of bubbles is different, and the distance r between the nearest-neighbor bubbles changes. In bubble phase A, the distance is $r = 2\sqrt{3}$, while in bubble phase B, $r = 4$. In bubble phase B the distance is larger, and the bubble density is lower, which increases the magnetization and reduces the Zeeman energy.

We also find two phases at low fields whose magnetic structure has a stripe frame of down spins with a one-stripe width [Figs. 4(a) and 4(b)]. We call these phases at lower and higher fields stripe phases A and B, respectively. In the two phases, the location of the down spins neighboring the stripe frame [blue circles in Figs. 4(c) and 4(d)] is different. We call these neighboring spins "branch spins." In the magnetic structure in stripe phase A illustrated in Fig. 4(a), the branch spins do not form a lattice and align randomly [Fig. 4(c)]. In stripe phase B, however, the branch spins form a triangular lattice [Fig. 4(d)].

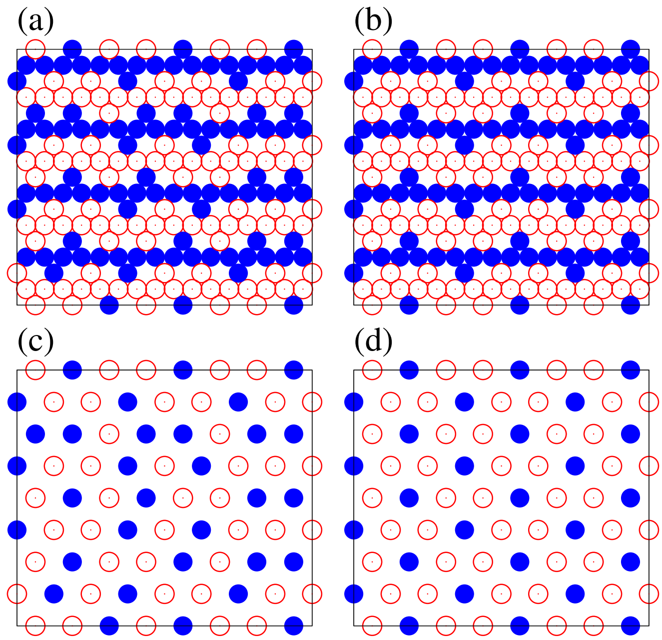

FIG. 4. Snapshots of the magnetic structure at $T = 0.05$ in the space-filling configuration (a) in stripe phase A at $H = 0.2$ and (b) in stripe phase B at $H = 0.6$. Snapshots of the magnetic structure of "branch spins"(c) in stripe phase A and (d) in stripe phase B. A $16\times8\sqrt{3}$ region is displayed. Blue solid and red open circles denote down and up spins, respectively. It should be noted that the branch spins in stripe phase B form a triangular lattice.

B. Bubble phases

We introduce several types of order parameters to study the phase transitions in the system. To investigate bubble phases A and B, we analyze the Fourier component of the spin configuration,

$$\bar{\varphi}_{\boldsymbol{k}} = \left\langle \left| \frac{1}{N} \sum_i \sigma_i e^{\boldsymbol{k}\cdot\boldsymbol{x}_i} \right| \right\rangle, \tag{3}$$

where $\langle \cdots \rangle$ denotes the thermal average.

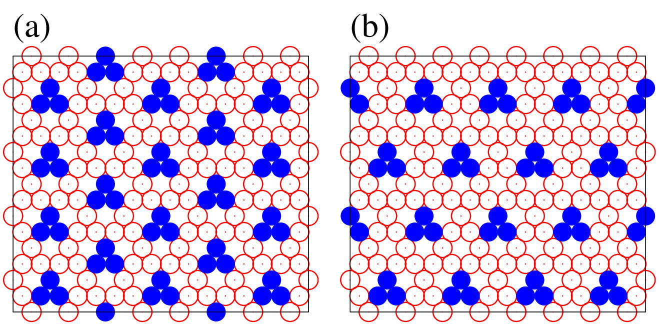

FIG. 3. Snapshots of the magnetic structure at $T = 0.05$ in the space-filling configuration (a) in bubble phase A at $H = 1.6$ and (b) in bubble phase B at $H = 2.3$. A $16\times8\sqrt{3}$ region is displayed. Blue solid and red open circles denote down and up spins, respectively.

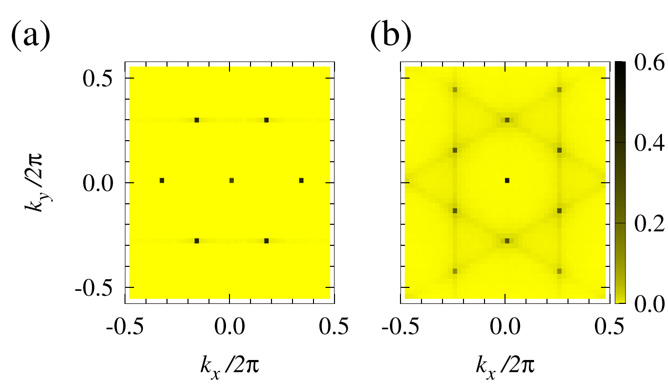

FIG. 5. $\bar{\varphi}_{\boldsymbol{k}}$ at $T = 0.05$ at (a) $H = 1.6$ and (b) $H = 2.3$.

In Figs. 5(a) and 5(b), we illustrate $|\bar{\varphi}_{\boldsymbol{k}}|$ at $H = 1.6$ and $H = 2.3$, respectively, at $T = 0.05$. The smallest reciprocal lattice vectors for the triangular lattice of bubbles in bubble phase A are $\boldsymbol{k}_1 = (\frac{2\pi}{3}, 0)$ and $\boldsymbol{k}'_1 = (-\frac{\pi}{3}, \frac{\sqrt{3}\pi}{3})$, and those in bubble phase B are $\boldsymbol{k}_2 = (0, \frac{\pi}{\sqrt{3}})$ and $\boldsymbol{k}'_2 = (\frac{\pi}{2}, -\frac{\sqrt{3}\pi}{6})$. We find that linear combinations of $\boldsymbol{k}_1$ and $\boldsymbol{k}'_1$ and those of $\boldsymbol{k}_2$ and $\boldsymbol{k}'_2$ correspond to the high-intensity parts (black spots) in Figs. 5(a) and 5(b), respectively. Hence, we define the order parameters for bubble phase A as

$$\varphi_1 = \left\langle \left| \frac{9}{4N} \sum_j \sigma_j e^{i\frac{2\pi}{3}x_j} \right| \right\rangle \tag{4}$$

and

$$\varphi'_1 = \left\langle \left| \frac{9}{4N} \sum_j \sigma_j e^{i(-\frac{\pi}{3}x_j + \frac{\sqrt{3}\pi}{3}y_j)} \right| \right\rangle \tag{5}$$

and those for bubble phase B as

$$\varphi_2 = \left\langle \left| \frac{6}{\sqrt{5}N} \sum_j \sigma_j e^{i\frac{\pi}{\sqrt{3}}y_j} \right| \right\rangle \tag{6}$$

and

$$\varphi'_2 = \left\langle \left| \frac{6}{\sqrt{5}N} \sum_j \sigma_j e^{i(\frac{\pi}{2}x_j - \frac{\sqrt{3}\pi}{6}y_j)} \right| \right\rangle. \tag{7}$$

Here, the prefactors $\frac{9}{4}$ and $\frac{6}{\sqrt{5}}$ are normalization constants.

We also study the magnetization of the system to characterize the regions of the ordered phases,

$$m_z = \left\langle \frac{1}{N} \sum_i^N \sigma_i \right\rangle, \tag{8}$$

and the sum of the Ising and dipolar interaction energies,

$$E = \left\langle \frac{1}{N} \left(-\delta \sum_{\langle i,j \rangle} \sigma_i \sigma_j + \sum_{i<j} \frac{\sigma_i \sigma_j}{r_{ij}^3} \right) \right\rangle. \tag{9}$$

We plot the H dependences at $T = 0.05$ of φ_1 and φ'_1 in Fig. 6(a) and of φ_2 and φ'_2 in Fig. 6(b). We find that bubble phase A appears at $1.1 \lesssim H \lesssim 1.9$ and bubble phase B appears at $2.2 \lesssim H \lesssim 2.5$. In these field regions, plateaus of m_z and E appear in Figs. 7 and 8, respectively, which indicates that the configurations in Figs. 3(a) and 3(b) are maintained. (Above $H = 3$, m_z monotonically increases and is saturated at $H \simeq 4.0$.)

We find that at $0.34 \lesssim H \lesssim 0.65$, φ_1 and φ'_1 appear but are much less than 1 and are accompanied by a plateau of m_z, and at $H \lesssim 0.65$, φ_2 and φ'_2 appear with a large fluctuation. We consider the reasons for these observations in the next section.

C. Stripe phases

Stripe phases of Ising dipolar systems have been studied mainly on a square lattice. There the numbers of horizontal (n_h) and vertical (n_v) bonds between nearest-neighbor antialigned spins are calculated, and the order parameter is defined as the difference between n_h and n_v, which indicates ($\pi/2$)-rotational symmetry breaking [21,25].

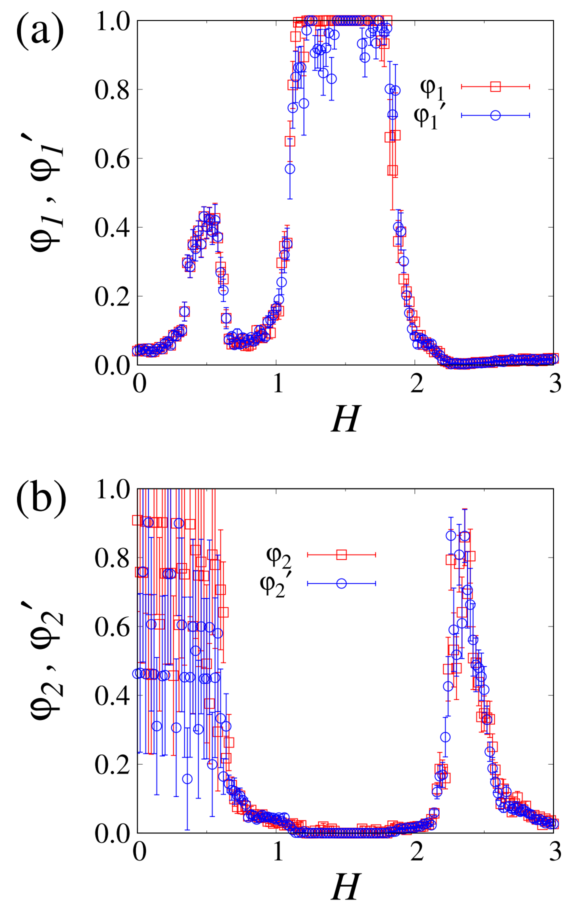

FIG. 6. H dependences at $T = 0.05$ of (a) φ_1 and φ'_1 and (b) φ_2 and φ'_2.

In the case of the kagome lattice, we should investigate ($\pi/3$)-rotational symmetry breaking to detect the stripe phases. There are three bond angles from the x axis concerning nearest-neighbor antialigned spin pairs, i.e., 0, $\frac{\pi}{3}$, and $\frac{2\pi}{3}$. We define the order parameter

$$O_{123} = 2\frac{|n_1 + n_2\omega + n_3\omega^2|}{|n_1 + n_2 + n_3|}. \tag{10}$$

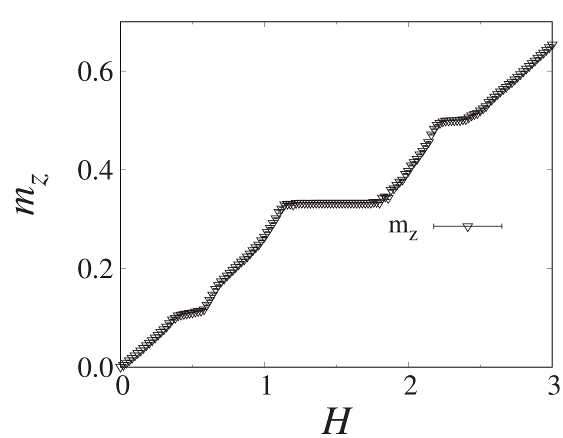

FIG. 7. H dependence of m_z at $T = 0.05$.

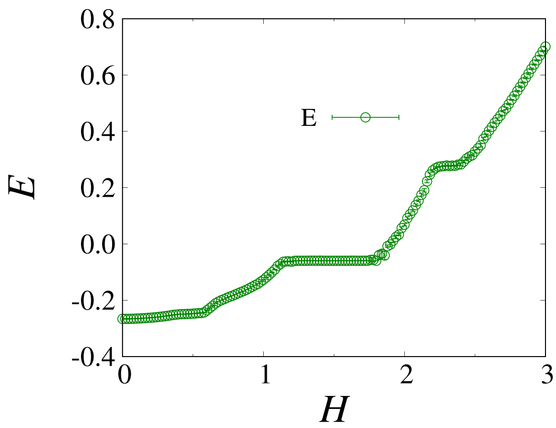

FIG. 8. H dependence of E at $T = 0.05$.

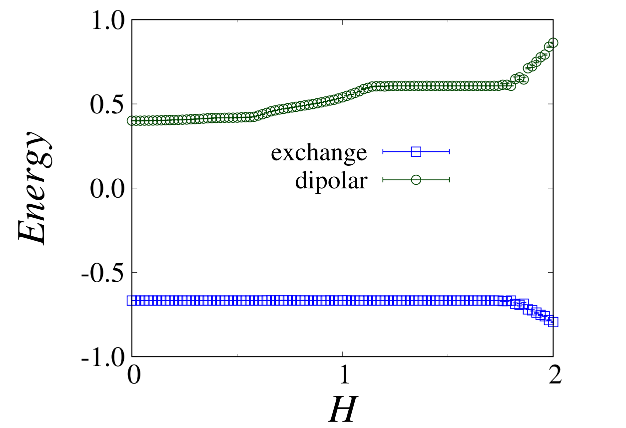

FIG. 10. H dependences of the exchange and dipolar interaction energies at $T = 0.05$.

Here, $\omega = e^{\frac{2\pi i}{3}}$, which satisfies $1 + \omega + \omega^2 = 0$, and n_1, n_2, and n_3 are the numbers of bonds of nearest-neighbor antialigned spins with bond angles of 0, $\frac{\pi}{3}$, and $\frac{2\pi}{3}$, respectively. The prefactor 2 is a normalization constant.

We present the H dependence of O_{123} in Fig. 9. We find that at $H \lesssim 0.65$, O_{123} reaches almost full saturation, and a stripe phase or stripe phases are identified in this region. The period of the stripes is $2\sqrt{3}$ [Figs. 4(a) and 4(b)], the horizontal stripes are detected by φ_2, and the diagonal stripes parallel to the direction of $(1, \sqrt{3})$ are detected by φ_2'. Therefore, finite values of φ_2 and φ_2' with fluctuation in Fig. 6 are ascribed to the formation of these stripes.

We find in Figs. 7 and 8 a plateaulike region of m_z and E at $0.34 \lesssim H \lesssim 0.65$, at which φ_1 and φ_1' have finite values (<0.5) in Fig. 6. This plateaulike region suggests that the structure of Fig. 4(b) is stable against the magnetic field. We notice that the branch spins in stripe phase B form a triangular lattice with lattice constant $2\sqrt{3}$, which is the same as that of the triangular bubble lattice in bubble phase A. The triangular lattice of the branch spins causes finite values of φ_1 and φ_1', which is evidence of the realization of stripe phase B at $0.34 \lesssim H \lesssim 0.65$.

We find that the exchange interaction energy, i.e., the first term of E, is constant for $H \lesssim 1.8$ (Fig. 10), including the regions of stripe phases A and B and bubble phase A. The constant exchange interaction energy is easily confirmed between the two stripe phases, and it is also confirmed between stripe phase B and bubble phase A by considering the transformations between Figs. 11(a) and 11(b) and between Figs. 11(b) and 11(c). It is interesting to note that in the field region of the disordered phase between stripe phase B and bubble phase A, the exchange interaction energy is unchanged, although disordered spin configurations such as that in Fig. 12 at $H = 0.9$ and $T = 0.05$ appear.

In the two stripe phases, because the exchange energy associated with branch spins is zero and thus the exchange energy originates only from the stripe part, the spin configuration of the branch spins is considered to be located on the triangular lattice with a lattice constant of $2\sqrt{3}$ only by the dipolar interaction and the magnetic field.

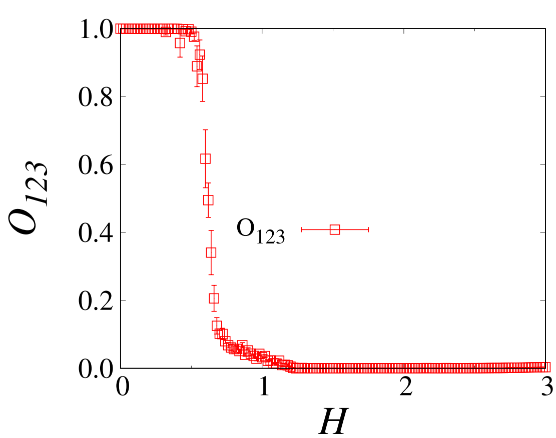

FIG. 9. H dependence of O_{123} at $T = 0.05$.

D. Phase transitions

We investigate the properties of phase transitions. In Fig. 13, φ_2 and φ_2' in a heating and cooling process at $H = 2.3$ are shown. We find thermal hysteresis loops of φ_2 and φ_2', which indicates the existence of metastable states between bubble phase B and the disordered phase. Therefore, the transition associated with these hysteresis loops is identified as a first-order transition. We adopt the middle point (temperature) of the loops as the first-order transition point and plot this point with a red circle in the phase diagram in Fig. 2, in which the error bar coincides with the loop width. In the same manner, first-order transition points between bubble phase B

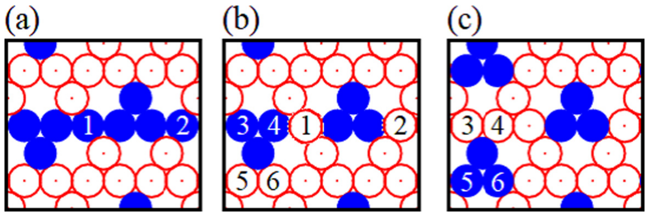

FIG. 11. Configurations with the same exchange interaction energy. The difference in the configuration between (a) and (b) is spins 1 and 2, and that between (b) and (c) is spins 3, 4, 5, and 6.

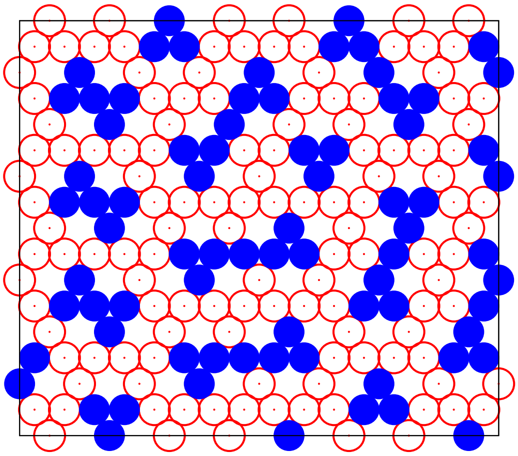

FIG. 12. Snapshot of the spin configuration at $H = 0.9$ and $T = 0.05$.

and the disordered phase are plotted with red circles on the phase diagram.

In Fig. 14, φ_1 and φ_1' in a heating and cooling process at $H = 1.6$ are presented. We find a very small hysteresis loops, but it is difficult to judge whether the transition is first order. Next, we perform an energy histogram analysis. If the phase transition is first order, the histogram should have two peaks around the transition temperature. We find double peaks around $T = 0.226$ in Fig. 15 and judge this point to be a first-order transition point between bubble phase A and the disordered phase. In the same manner, the first-order transition point at $H = 1.4$ is determined. These first-order transition points are plotted by red circles between bubble phase A and the disordered phase on the phase diagram.

We find points around phase boundaries at which neither hysteresis loops nor double peaks of the energy histogram have been observed within the accuracy of the present work and study the heat capacity per spin for several such points,

$$C = \frac{1}{N}\frac{\langle E_t^2\rangle - \langle E_t\rangle^2}{k_B T^2}, \tag{11}$$

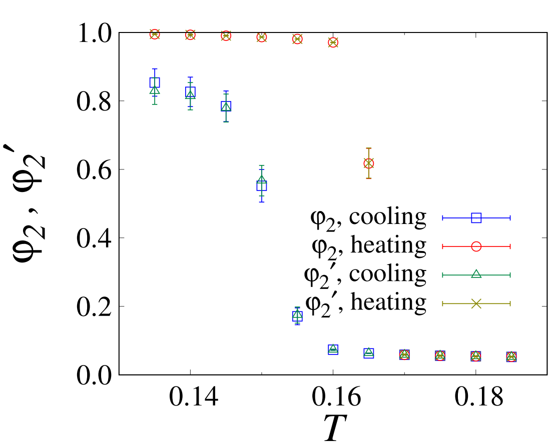

FIG. 13. φ_2 and φ_2' in the heating and cooling process at $H = 2.3$. Hysteresis loops of φ_2 and φ_2' are observed.

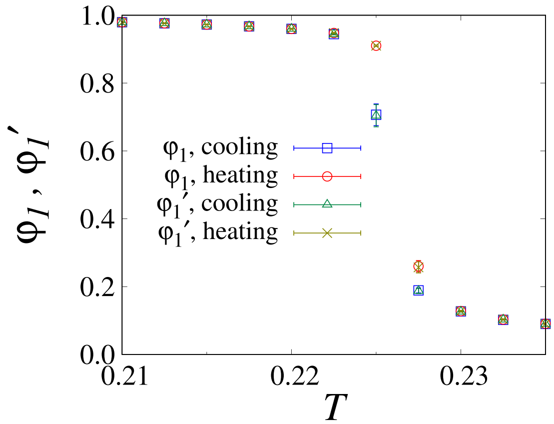

FIG. 14. φ_1 and φ_1' in the heating and cooling process at $H = 1.6$.

where E_t is the total energy of the system. In Figs. 16(a) and 16(b), we give the temperature dependence of the heat capacity at $H = 0.0$, 0.2, 0.4, and 0.6 for $0.12 < T < 0.2$ and at $H = 0.4$ and 0.6 for $0.07 < T < 0.12$, respectively. The peaks of C in Fig. 16(a) show the transition points between stripe phase A and the disordered phase, while the peaks of C at $H = 0.4$ and 0.6 in Fig. 16(b) give the transition points between stripe phases A and B. These points are plotted with solid squares on the phase diagram.

We also analyze the temperature dependence of C at $H = 1.2$ and 1.8 between bubble phase A and the disordered phase and find peaks. These points are also plotted with solid squares on the phase diagram. Considering the first-order transition points (red circles) at $H = 1.4$ and 1.6, these transitions are of weak first order.

In our previous study on a square lattice [34], the transition between the stripe and disordered phases at low H was second order. Here, to investigate the possibility of a second-order transition, we calculate the Binder cumulant U_4 of O_{123} at low fields,

$$U_4 = 1 - \frac{\langle O_{123}^4\rangle}{3\langle O_{123}^2\rangle^2}. \tag{12}$$

In Fig. 17, the Binder cumulants at $H = 0$ for different system sizes are plotted. We find no crossing of these cumulants and

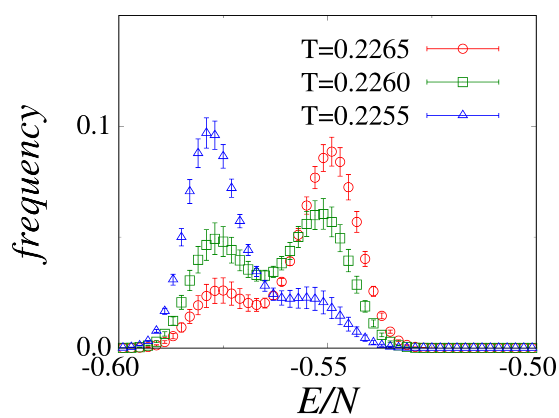

FIG. 15. Energy histograms at $H = 1.6$ at $T = 0.2265$, 0.226, and 0.2255.

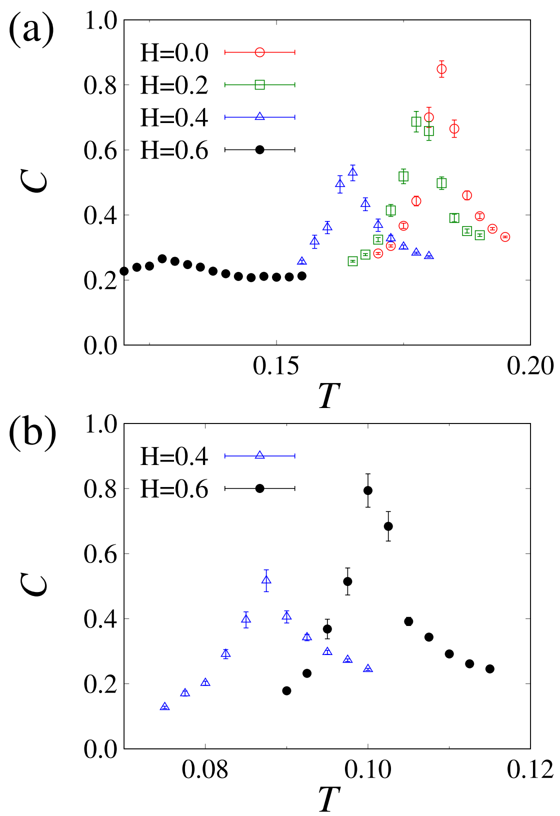

FIG. 16. Temperature dependence of heat capacity at (a) $H = 0.0$, 0.2, 0.4, and 0.6 for $0.12 < T < 0.2$ and at (b) $H = 0.4$ and $H = 0.6$ for $0.07 < T < 0.12$.

observe the same tendency at solid squares at $H = 0.2$ and 0.4 on the phase diagram, and we judge that the phase transition between stripe phase A and the disordered phase is not second order.

We show the phase boundaries at $T = 0.05$ by open squares in the phase diagram based on the H dependences of the order parameters (Figs. 6, 7, and 9). In the same manner, the other open squares are plotted using the H dependences of the order parameters at $T = 0.1$ and $T = 0.15$. We find that a disordered phase exists between stripe phase B (or A) and bubble phase A, between bubble phases A and B, and above bubble phase B, and the phase boundaries at low temperatures extend to higher temperatures in the T direction.

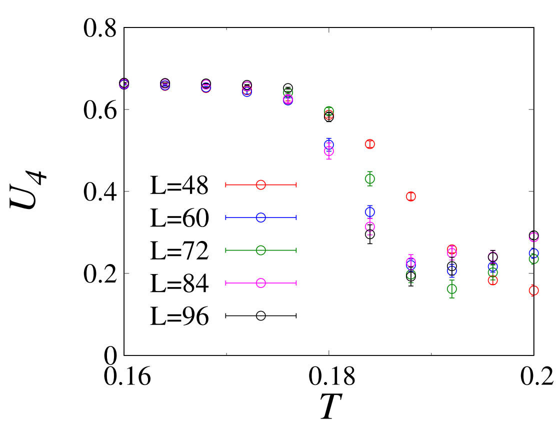

FIG. 17. Temperature dependence of the Binder cumulant at $H = 0$.

IV. DISCUSSION AND SUMMARY

Studies on bubble formation using lattice models were limited to square lattices, as mentioned in the Introduction. They showed a stripe phase (phases) at low fields and a bubble phase at high fields. The stripe phase did not have branch spins, and bubbles did not show a lattice structure, namely, structure with no apparent symmetry. However, the kagome-lattice dipolar Ising ferromagnet in this study presented two bubble phases with high symmetry, i.e., a triangular lattice. Furthermore, branch spins neighboring the stripe frame change the symmetry with the field. Higher symmetry, i.e., a triangular lattice of branch spins, is realized at higher fields. This is also a unique feature of the kagome-lattice dipolar Ising ferromagnet. The two bubble phases are robust against the variation of the external magnetic field. In each bubble phase, the configuration, magnetization, and total energy except the Zeeman term remain. The origin of these unique features may be attributed to the defect effect, and the symmetry of the bubble phase may reflect that of the defect. Our study suggests that the defect can stabilize bubbles and the symmetry of the defects may determine those of bubbles and branch spins in dipolar Ising ferromagnets.

A limited number of 2D Ising ferromagnets have been reported, such as $BaFe_2(PO_4)_2$ [57] and CrI_3 [58], in which the out-of-plane magnetization shows an order-disorder transition on a honeycomb lattice. If the dipolar interaction is relatively strong compared with the exchange interaction, the dipolar interaction becomes important. The effect of the dipolar interaction on a honeycomb-lattice Ising ferromagnet was studied using a Monte Carlo method [31], which suggested properties similar to those of dipolar square-lattice Ising ferromagnets. On the other hand, kagome-lattice Ising ferromagnets have not been reported yet. Considering recent developments in experimental techniques for making artificial lattices such as artificial kagome dipolar spin ice, realized by connected Co nanomagnets [52,53], kagome Ising ferromagnets might not be imaginary systems in the future. Regardless of this realization, the defect effect in this study will be useful for insights into how to control magnetic structures in systems with competition between short- and long-range interactions.

We summarize the present study below. We investigated the two-dimensional dipolar Ising ferromagnet on a kagome lattice with a specific ratio between the exchange and dipolar constants, $\delta = 1$. We calculated the order parameters for bubbles and stripes and other thermodynamic quantities using the stochastic cutoff $O(N)$ Monte Carlo method and analyzed the field-temperature phase diagram.

We found two stripe phases at low fields, where the stripe frame has a one-stripe width. In the lower-field stripe phase (stripe phase A), the branch spins, defined as reversed spins neighboring the stripe frame, align randomly, while in the higher-field stripe phase (stripe phase B), the branch spins form a triangular lattice, which shows a magnetization plateau. In stripe phase A, the magnetization changes with increasing the field, but the exchange interaction energy is constant in both stripe phases A and B, where the dipolar interaction is essential in the formation of the magnetic structure of the branch spins.

We also found two bubble phases at high fields. In both bubble phases, three nearest-neighbor down spins form a triangular domain, i.e., bubble, and bubbles form a triangular lattice, but the triangular array of bubbles and distance between bubbles vary. Interestingly, the exchange energy is constant not only in the two stripe phases but also in the lower-field bubble phase (bubble phase A) and intermediate disordered phase.

We determined the phase boundaries and showed several properties of the phase transitions. So far, a first-order transition has been suggested between stripe and bubble phases. However, a specific lattice structure was assumed in the effective free-energy approaches, and bubble phases were studied without defining an order parameter for a lattice structure. In this paper we defined the bubble phase as a phase with a lattice structure formed by magnetic domains. Consequently, we discovered that a disordered phase exists between stripe A (B) and bubble phase A and between the two bubble phases, and the transitions between the two bubble phases and disordered phase are first order at high temperatures.

ACKNOWLEDGMENTS

The present study was supported by Grants-in-Aid for Scientific Research C (Grants No. 18K03444 and No. 20K03809) from the Ministry of Education, Culture, Sports, Science and Technology (MEXT) of Japan and the Elements Strategy Initiative Center for Magnetic Materials (ESICMM; Grant No. 12016013) funded by MEXT. The calculations were partially performed using the Numerical Materials Simulator (supercomputer) at the National Institute for Materials Science.

APPENDIX: SCO ALGORITHM FOR THE ISING DIPOLAR MODEL

In the original SCO algorithm, the stochastic potential switching (SPS) procedure [59,60] with $O(N)$ switching time is applied to all long-range interactions in the system. In the case of Ising spins, however, the application of the SCO method to neighboring spins causes a delay in the relaxation time, and a tuning of the number of dipolar interactions to which the SPS procedure is applied is necessary to accelerate the relaxation time. In the present study, we tune the number of dipolar interactions using a Metropolis algorithm for the dipolar interactions which satisfy $|\mu_i - \mu_j| \leqslant 5$ and $|\nu_i - \nu_j| \leqslant 5$ and the SCO algorithm for the dipolar interactions outside this region.

In the SPS algorithm long-range interaction V_{ij} is stochastically switched to $\tilde{V}_{ij}$ with a probability P_{ij} or to $\bar{V}_{ij}$ with $1 - P_{ij}$. The potential $\tilde{V}_{ij}$ can be chosen arbitrarily. Here, P_{ij} is written as

$$P_{ij}(\sigma_i, \sigma_j) = \exp[\beta(\Delta V_{ij}(\sigma_i, \sigma_j) - \Delta V_{ij}^*)], \tag{A1}$$

where

$$\Delta V_{ij}(\sigma_i, \sigma_j) = V_{ij}(\sigma_i, \sigma_j) - \tilde{V}_{ij}(\sigma_i, \sigma_j) \tag{A2}$$

and ΔV_{ij}^* is a constant equal to or greater than the maximum value of ΔV_{ij}. The potential $\bar{V}_{ij}$ is given by

$$\bar{V}_{ij}(\sigma_i, \sigma_j) = V_{ij}(\sigma_i, \sigma_j) - \beta^{-1} \ln[1 - P_{ij}(\sigma_i, \sigma_j)]. \tag{A3}$$

Here, $\tilde{V}_{ij} = 0$ is set, and the computational time is reduced to $O(N)$ for dipolar spin systems [56]. This procedure works well for dipolar Heisenberg systems [54,56,61].

However, some modification is useful for dipolar Ising systems. This improvement is attributed to the discretized spin state (up or down) of the Ising spin. The dipolar interaction,

$$V_{ij}(\sigma_i, \sigma_j) = \frac{\sigma_i \sigma_j}{r_{ij}^3}, \tag{A4}$$

takes two values, i.e., $V_{ij}(\sigma_i, \sigma_j) = \frac{1}{r_{ij}^3}$ and $-\frac{1}{r_{ij}^3}$ for ferromagnetic ($\sigma_i = \sigma_j = \pm 1$) and antiferromagnetic ($\sigma_i = -\sigma_j = \pm 1$) spins, respectively. Defining $\Delta V_{ij}^* = \alpha \frac{1}{r_{ij}^3}$, in which $\alpha > 1$, $P_{ij}(\sigma_i, \sigma_j) = \exp(\frac{1-\alpha}{r_{ij}^3 T})$, and $\exp(\frac{-1-\alpha}{r_{ij}^3 T})$ for ferromagnetic and antiferromagnetic spins, respectively. In the present study we take $\alpha = 1.5$.

Because

$$\frac{P_{ij}(\sigma_i = 1, \sigma_j = 1)}{P_{ij}(\sigma_i = 1, \sigma_j = -1)} = \exp\left(\frac{2}{r_{ij}^3 T}\right), \tag{A5}$$

P_{ij} for ferromagnetic spins is much larger than that for antiferromagnetic spins for smaller r_{ij} and lower T. The probability for selecting $\bar{V}_{ij}$ for ferromagnetic spins is much smaller than that for antiferromagnetic spins. This large difference in $P_{ij}(\sigma_i, \sigma_j)$ causes a deviation in the potential switching pattern and inefficiency in the MC sampling. Therefore, we use a Metropolis algorithm instead of the SCO algorithm for spin pairs of the dipolar interaction within a short distance. The efficiency of this method was previously studied for a dipolar Ising model on a square lattice in Ref. [34].

[1] *Ultrathin Magnetic Structures*, edited by B. Heinrich and J. A. C. Bland (Springer, Berlin, 2004).
[2] S. D. Bader, Rev. Mod. Phys. **78**, 1 (2006).
[3] D. P. Pappas, K.-P. Kämper, and H. Hopster, Phys. Rev. Lett. **64**, 3179 (1990).
[4] R. Allenspach and A. Bischof, Phys. Rev. Lett. **69**, 3385 (1992).
[5] R. Ramchal, A. K. Schmid, M. Farle, and H. Poppa, Phys. Rev. B **69**, 214401 (2004).
[6] C. Won, Y. Z. Wu, J. Choi, W. Kim, A. Scholl, A. Doran, T. Owens, J. Wu, X. F. Jin, H. W. Zhao, and Z. Q. Qiu, Phys. Rev. B **71**, 224429 (2005).
[7] Z. Q. Qiu, J. Pearson, and S. D. Bader, Phys. Rev. Lett. **70**, 1006 (1993).
[8] X. Z. Yu, Y. Onose, N. Kanazawa, J. H. Park, J. H. Han, Y. Matsui, N. Nagaosa, and Y. Tokura, Nature (London) **465**, 901 (2010).

[9] J. A. Cape and G. W. Lehman, J. Appl. Phys. **42**, 5732 (1971).
[10] A. Hubert and R. Schäfer, *Magnetic Domains* (Springer, Berlin, 1998).
[11] M. Seul and D. Andelman, Science **267**, 476 (1995).
[12] T. Garel and S. Doniach, Phys. Rev. B **26**, 325 (1982).
[13] A. Mendoza-Coto, O. V. Billoni, S. A. Cannas, and D. A. Stariolo, Phys. Rev. B **94**, 054404 (2016).
[14] S. A. Cannas, M. Carubelli, O. V. Billoni, and D. A. Stariolo, Phys. Rev. B **84**, 014404 (2011).
[15] R. Díaz-Méndez and R. Mulet, Phys. Rev. B **81**, 184420 (2010).
[16] V. L. Berezinskii, Sov. Phys. JETP **32**, 493 (1971); **34**, 610 (1972).
[17] J. M. Kosterlitz and D. J. Thouless, J. Phys. C **6**, 1181 (1973).
[18] B. I. Halperin and D. R. Nelson, Phys. Rev. Lett. **41**, 121 (1978).
[19] D. R. Nelson and B. I. Halperin, Phys. Rev. B **19**, 2457 (1979).
[20] A. P. Young, Phys. Rev. B **19**, 1855 (1979)
[21] I. Booth, A. B. MacIsaac, J. P. Whitehead, and K. De'Bell, Phys. Rev. Lett. **75**, 950 (1995).
[22] A. B. MacIsaac, J. P. Whitehead, M. C. Robinson, and K. De'Bell, Phys. Rev. B **51**, 16033 (1995).
[23] J. H. Toloza, F. A. Tamarit, and S. A. Cannas, Phys. Rev. B **58**, R8885 (1998).
[24] E. Rastelli, S. Regina, and A. Tassi, Phys. Rev. B **73**, 144418 (2006).
[25] S. A. Cannas, M. F. Michelon, D. A. Stariolo, and F. A. Tamarit, Phys. Rev. B **73**, 184425 (2006).
[26] S. A. Pighin and S. A. Cannas, Phys. Rev. B **75**, 224433 (2007).
[27] E. Rastelli, S. Regina, and A. Tassi, Phys. Rev. B **76**, 054438 (2007).
[28] A. Vindigni, N. Saratz, O. Portmann, D. Pescia, and P. Politi, Phys. Rev. B **77**, 092414 (2008).
[29] L. G. Rizzi and N. A. Alves, Phys. B (Amsterdam, Neth.) **405**, 1571 (2010).
[30] J. S. M. Fonseca, L. G. Rizzi, and N. A. Alves, Phys. Rev. E **86**, 011103 (2012).
[31] R. Rüger and R. Valentí, Phys. Rev. B **86**, 024431 (2012).
[32] C. M. Horowitz, M. A. Bab, M. Mazzini, M. L. Rubio Puzzo, and G. P. Saracco, Phys. Rev. E **92**, 042127 (2015).
[33] M. A. Bab, C. M. Horowitz, M. L. Rubio Puzzo, and G. P. Saracco, Phys. Rev. E **94**, 042104 (2016).
[34] H. Komatsu, Y. Nonomura, and M. Nishino, Phys. Rev. E **98**, 062126 (2018).
[35] D. Pescia and V. L. Pokrovsky, Phys. Rev. Lett. **65**, 2599 (1990).
[36] A. Moschel and K. D. Usadel, J. Magn. Magn. Mater. **140–144**, 649 (1995).
[37] A. Hucht, A. Moschel, and K. D. Usadel, J. Magn. Magn. Mater. **148**, 32 (1995).
[38] A. B. MacIsaac, J. P. Whitehead, K. De'Bell, and P. H. Poole, Phys. Rev. Lett. **77**, 739 (1996).
[39] A. B. MacIsaac, K. De'Bell, and J. P. Whitehead, Phys. Rev. Lett. **80**, 616 (1998).
[40] K. De'Bell, A. B. MacIsaac, and J. P. Whitehead, Rev. Mod. Phys. **72**, 225 (2000).
[41] C. Santamaria and H. T. Diep, J. Magn. Magn. Mater. **212**, 23 (2000).
[42] M. Rapini, R. A. Dias, and B. V. Costa, Phys. Rev. B **75**, 014425 (2007).
[43] J. P. Whitehead, A. B. MacIsaac, and K. De'Bell, Phys. Rev. B **77**, 174415 (2008).
[44] M. Carubelli, O. V. Billoni, S. A. Pighin, S. A. Cannas, D. A. Stariolo, and F. A. Tamarit, Phys. Rev. B **77**, 134417 (2008).
[45] L. A. S. Mól and B. V. Costa, Phys. Rev. B **79**, 054404 (2009).
[46] S. A. Pighin, O. V. Billoni, D. A. Stariolo, and S. A. Cannas, J. Magn. Magn. Mater. **322**, 3889 (2010).
[47] S. A. Pighin, O. V. Billoni, and S. A. Cannas, Phys. Rev. E **86**, 051119 (2012).
[48] L. A. S. Mól and B. V. Costa, J. Magn. Magn. Mater. **353**, 11 (2014).
[49] H. Komatsu, Y. Nonomura, and M. Nishino, Phys. Rev. B **100**, 094407 (2019).
[50] H. Komatsu, Y. Nonomura, and M. Nishino, Phys. Rev. B **103**, 214404 (2021).
[51] S. T. Bramwell and M. J. P. Gingras, Science **294**, 1495 (2001).
[52] N. Rougemaille, F. Montaigne, B. Canals, A. Duluard, D. Lacour, M. Hehn, R. Belkhou, O. Fruchart, S. El Moussaoui, A. Bendounan, and F. Maccherozzi, Phys. Rev. Lett. **106**, 057209 (2011).
[53] B. Canals, I.-A. Chioar, V.-D. Nguyen, M. Hehn, D. Lacour, F. Montaigne, A. Locatelli, T. O. Mentes, B. S. Burgos, and N. Rougemaille, Nat. Commun. **7**, 11446 (2016).
[54] Y. Tomita, J. Phys. Soc. Jpn. **78**, 114004 (2009).
[55] M. S. Holden, M. L. Plumer, I. Saika-Voivod, and B. W. Southern, Phys. Rev. B **91**, 224425 (2015).
[56] M. Sasaki and F. Matsubara, J. Phys. Soc. Jpn. **77**, 024004 (2008).
[57] R. David, A. Pautrat, D. Filimonov, H. Kabbour, H. Vezin, M.-H. Whangbo, and O. Mentré, J. Am. Chem. Soc. **135**, 13023 (2013).
[58] B. Huang, G. Clark, E. Navarro-Moratalla, D. R. Klein, R. Cheng, K. L. Seyler, D. Zhong, E. Schmidgall, M. A. McGuire, D. H. Cobden, W. Yao, D. Xiao, P. Jarillo-Herrero, and X. Xu, Nature (London) **546**, 270 (2017).
[59] C. H. Mak, J. Chem. Phys. **122**, 214110 (2005).
[60] C. H. Mak and A. K. Sharma, Phys. Rev. Lett. **98**, 180602 (2007).
[61] T. Hinokihara, M. Nishino, Y. Toga, and S. Miyashita, Phys. Rev. B **97**, 104427 (2018).